Further Developments in Consistent Unsteady Supersonic Aerodynamic Coefficients

KARIAPPA* AND G. C. C. SMITH†
Bell Aerospace Company, Division of Textron, Buffalo, N.Y.

A finite element method to evaluate unsteady supersonic aerodynamic coefficients consistent with structural stiffness and inertia properties of a lifting surface is described. The grid and element system on the wing surface can be the same as in the structural analysis. Partial elements at wing and diaphragm edges are avoided, and downwash continuity is maintained, thereby yielding improved pressure distributions. Use of quadratic interpolation of velocity potentials and displacements improves accuracy, or leads to the necessity for fewer elements. Numerical results are obtained for several wing planforms at various Mach Numbers and reduced frequencies, and are compared with other methods.

Nomenclature

$\mathbf{a}$	= Boolean matrix describing topological connections of the elements in the structure
$\mathbf{A}, \mathbf{B}$	= aerodynamic influence coefficient matrices
l	= a reference length
M	= Mach number
$\mathbf{P}$	= column vector of nodal forces
$\mathbf{q}$	= column vector of displacements
R, S, r, s	= oblique coordinates
t	= dimensional time
U	= forward speed
w	= downwash
$X - x, y$	= position vector of receiving point
$\Xi = \xi, \eta$	= position vector of influencing point
z	= normal displacement within an element
α	= damping factor
$\zeta_1, \zeta_2, \zeta_3$	= homogeneous coordinates
k	= complex reduced frequency
$\bar{\lambda} = [(\alpha l/U) + i(\omega l/U)]$	= complex eigenvalue
$\boldsymbol{\rho}$	= kinematic mode vector
ρ	= density of air
$\boldsymbol{\phi}$	= column vector of velocity potential
$\boldsymbol{\Phi}$	= velocity potential influence coefficient
$\boldsymbol{\Omega}$	= transformation matrix
ω	= circular frequency

Subscripts

i, j	= receiving and influencing elements, respectively
x, ξ	= derivative with respect to x and ξ, respectively

Introduction

THE avoidance of aeroelastic instabilities and the reduction of aeroelastic effects to acceptable or desirable levels are major considerations in the design of flight vehicles. The aeroelastic phenomenon is an interaction of elastic, inertial and aerodynamic forces. Determination of these forces and methods of solution of the resulting equations are subjects of continuing development.

Presented as Paper 71-177 at the AIAA 9th Aerospace Sciences Meeting, New York, January 25-27, 1971; submitted February 19, 1971; revision received September 2, 1971. This work was funded as IR&D by Bell Aerospace Company.

Index categories: Aeroelasticity and Hydroelasticity; Nonsteady Aerodynamics; and Supersonic and Hypersonic Flow.

*Senior Engineer.

†Chief Engineer, Structural Dynamics.

Computation of structural stiffness, inertia and modal properties has reached a high degree of versatility and accuracy with the aid of finite element techniques and high-speed digital computers. Evaluation of unsteady aerodynamic forces, with more involved fluid mechanics and boundary conditions, has remained largely isolated from structural aspects of the complete aeroelastic problem. On larger and faster vehicles, the aerodynamic terms in the unsteady equations become dominant. It is therefore necessary to maintain efforts to improve their estimation. Recent suggestions for active suppression of flutter type instabilities (modal control) and of gust response characteristics emphasize this need.

Traditional Methods

Mathematical approaches for the pressure distribution on oscillating wings in supersonic flow may be broadly classified as: 1) The method of acceleration potential relating downwash and pressure distribution (e.g. Ref. 5). 2) The method of source pulse distributions, relating downwash and source strength in velocity potential distribution (e.g. Refs. 1-4). Owing to difficulties in choosing pressure distribution functions the former method has not been popular. However, in Ref. 5; Cunningham has proposed the selection of more accurate series for lift distribution in the supersonic kernel function method. The method of source pulse distribution was first proposed by Garrick and Rubinow (Refs. 1 and 2). Closed form solutions have been established for simple planforms such as rectangular, tapered and delta wings. These exact solutions serve as standards for approximate methods developed for use on configurations more complex in planform and downwash distribution.

Numerical Methods

For more complex configurations such as swept and tapered wings, intersecting and control surfaces, numerical methods to compute aerodynamic coefficients have necessarily been developed. Most methods divide the 'integrating area' into a number of discrete 'panels' (e.g., square, Mach and characteristic boxes). Many of these methods assume constant source/downwash distribution over the panel or box. Leading and trailing edges, and Mach lines are then substituted by discontinuous or 'jagged' lines following box edges. Zartarian and Hsu have, in Ref. 6, discussed in detail the merits and demerits of individual box schemes and appropriate rules.

Currently, various developments of these methods are being made to improve the unsatisfactory pressure distributions caused by the jagged edge representation of the problem boundaries and the assumptions of piecewise constant downwash (Ref. 7 and 8).

Finite Element Method

Reference 10, using the source pulse concept of Refs. 1, 2, and a finite element model akin to current structural philosophy, proposed the derivation of kinematically consistent unsteady aerodynamic coefficients. This method has the following advantages: 1) On the lifting surface the grid system remains unchanged as Mach number varies, and can be the same as that used for structural analysis. 2) Diaphragm elements may be chosen independently of wing elements so as to minimize the computational effort or to obtain maximum efficiency in overall problems (unlike most box schemes in which the diaphragm elements are fixed by the number of boxes in the wing chord). 3) There are no partial elements either on the boundary of the lifting surface or on the front Mach lines (accepting piece-wise straight-line approximation to the wing planform). 4) Continuous downwash distribution is incorporated by representing the deformation of the elements by kinematic modes as used in structural analysis. 5) The virtual work principle results in the derivation of nodal forces consistent with the structural elastic and inertia forces, and facilities the direct formulation of nodal equations of motion if these are required; (for optimization for flutter conditions, for example).

In the examples of Ref. 10, linear variations of displacement and velocity potential within the triangular element were used to illustrate the improvement obtained in pressure distributions. For a given number of elements, accuracy may further be improved by quadratic interpolation of displacements and velocity potential. Lift and moment distribution on triangular wings and generalized aerodynamic coefficients for an AGARD planform have been calculated using quadratic interpolation functions. In this paper some comparisons are made between this approach and existing results using exact and box scheme methods.

Generalized Forces Using Consistent Matrices of Triangular Elements

Formulation of Element Influence Coefficients and Generalized Force Assembly

General finite element aerodynamic matrix derivation, and assembly and formulation of dynamical matrices are discussed in detail in Ref. 10. For the sake of completeness, application to triangular elements is briefly outlined. Triangular elements are commonly used in wing structural analysis since they fit well into general planforms. A simple example is given in Fig. 1. The elements can be in any orientation and of varying sizes. Deformation of the element can be expressed as a linear combination of rigid body motions and straining modes, such as stretching and rotations.[9] Reference 11 was such an application for panel flutter. For general structures, however, retention of all linear and rotational degrees of freedom increases the size of the eigenvalue problem while resulting in only second-order corrections to the eigenvalues. Similarly, retaining rotational degrees of freedom only maintains second-order consistency in the aerodynamic coefficients. Hence, in order to minimize computational effort, (not as a necessary condition for this method), all structural and aerodynamic forces will be expressed in terms of the nodal linear displacements. The internal displacement of the triangular element in this formulation will then be expressed by quadratic interpolation of the nodal linear displacements.

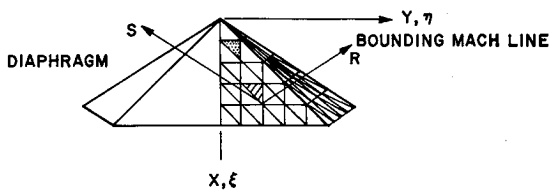

Fig. 1. Coordinate system and idealization of a typical wing.

The solution[2] to the potential-downwash equation of an arbitrarily oscillating surface in supersonic flow which lies in the plane $z = 0$ is

$$\phi(X,t) = \frac{-1}{\pi} \iint_S F(X,\Xi) w(\Xi,t) d\xi d\eta \tag{1}$$

where

$$F = \frac{\exp(-\lambda M^2/U\beta^2)(x-\xi)\cosh(\lambda M/U\beta^2)\,(r.s)^{1/2}}{(r.s)^{1/2}} \tag{2}$$

in which the hyperbolic radii are

$$r = (x-\xi) - \beta(y-\eta), \qquad s = (x-\xi) + \beta(y-\eta) \tag{3}$$

and the downwash w is given by

$$w = \left(\frac{\partial}{\partial t} + U\frac{\partial}{\partial \xi}\right) z(\Xi,t) \tag{4}$$

in which z is the deflection at the point $\Xi = (\xi, \eta, 0)$.

The integration indicated in Eq. (1) is taken over that area in front of the fore Mach cone of the point X. In the finite element idealization this area will be divided into a number of triangular elements. Thus, summing over all the elements, the velocity potential at X is given by

$$\phi_i(X) = \sum_j \phi_{ij} = -\frac{1}{\pi} \sum \iint_{S_j} F_{ij} w_j d\xi d\eta \tag{5}$$

where the subscript j denotes the influencing element, the subscript i the receiving element. Let $\mathbf{q}$ be the displacement vector of the complete structure. Then the displacement vector ρ for the jth element is a subset of $\mathbf{q}$ i.e.,

$$\rho_j = \mathbf{a}_j \mathbf{q} \tag{6}$$

where $\mathbf{a}$ is a Boolean matrix, which consists of zeroes and ones[9]. (The computer stores only the coordinates of ones and operates as additions or subtractions only and not as multiplications). Further, define $\boldsymbol{\Omega}$ as a quadratic interpolation matrix function expressed in terms of homogeneous coordinates[9] (see Fig. 2).

$$\underset{(1\times 6)}{\boldsymbol{\Omega}} = [\zeta_1(2\zeta_1 - 1),\ \zeta_2(2\zeta_2 - 1),\ \zeta_3(2\zeta_3 - 1),\ 4\zeta_1\zeta_2,\ 4\zeta_2\zeta_3,\ 4\zeta_3\zeta_1] \tag{7}$$

The relation between the rectangular and homogeneous coordinates is given by

$$\begin{Bmatrix} x \\ y \\ 1 \end{Bmatrix} = \begin{bmatrix} x_1 & x_2 & x_3 \\ y_1 & y_2 & y_3 \\ 1 & 1 & 1 \end{bmatrix} \begin{Bmatrix} \zeta_1 \\ \zeta_2 \\ \zeta_3 \end{Bmatrix} \tag{8}$$

Then the typical deflection within the jth element for an arbitrary motion is

$$z_j = \boldsymbol{\Omega} \rho_j e^{\lambda t} \tag{9}$$

and the downwash term

$$w_j = \left(\frac{U}{l}\right) [\bar{\lambda}\boldsymbol{\Omega} + \boldsymbol{\Omega}_\xi] \rho_j e^{\lambda t} \tag{10}$$

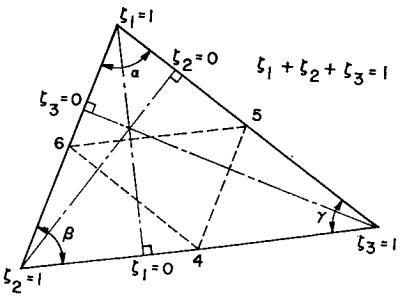

Fig. 2. Homogenous coordinates for a triangle.

where

$$\bar{\lambda} = \left(\frac{\alpha l}{U} + i\frac{\omega l}{U}\right)$$

is a complex reduced frequency.

From here it is convenient to assume all the space coordinates normalized with respect to l. Also subscripts to Ω will denote partial derivation, i.e.

$$\Omega_x = \frac{\partial \Omega}{\partial x} = \sum_{i=1}^{3} \frac{\partial \Omega}{\partial \zeta_i}\frac{\partial \zeta_i}{\partial x} \tag{11}$$

In the present analysis, the velocity potential will be evaluated with respect to the nodal points of the receiving triangle. Velocity potential within the triangle will then be interpolated quadratically. Using the linearized Bernoulli's expression, the pressure distribution can be established within the element. Finally, by the principle of virtual work the kinematically consistent aerodynamic influence coefficient matrix can be derived. Thus, the aerodynamic matrix for the element i due to perturbation in the element j can be written as,[10]

$$\mathbf{A}_{ij} = \frac{2\rho U^2 l^2}{\pi}\left[\mathbf{B}\Phi_b + \bar{\lambda}(\mathbf{B}\Phi_a + \mathbf{A}\Phi_b) + \bar{\lambda}^2\mathbf{A}\Phi_a\right]_{ij} \tag{12}$$

where

$$\Phi_{aij} = 2\Delta_j \int_0^1 \int_0^{1-\zeta_1} F_{ij}\Omega d\zeta_2 \zeta_1 \tag{13}$$

$$\Phi_{bij} = 2\Delta_j \int_0^1 \int_0^{1-\zeta_1} F_{ij}\Omega_\zeta d\zeta_2 d\zeta_1 \tag{14}$$

$$\mathbf{A} = 2\Delta_i \int_0^1 \int_0^{1-\zeta_1} \Omega_i{}^T \Omega_i d\zeta_2 d\zeta_1 \tag{15}$$

and

$$\mathbf{B} = 2\Delta_i \int_0^1 \int_0^{1-\zeta_1} \Omega_i{}^T \Omega_{xi} d\zeta_2 d\zeta_1 \tag{16}$$

Matrices **A** and **B** are given in Tables 1 and 2.

Table 1. *A* **matrix**

$$\begin{bmatrix}
\frac{1}{60} & \frac{-1}{360} & \frac{-1}{360} & 0 & \frac{-1}{90} & 0 \\
\frac{-1}{360} & \frac{1}{60} & \frac{-1}{360} & 0 & 0 & \frac{-1}{90} \\
\frac{-1}{360} & \frac{-1}{360} & \frac{1}{60} & \frac{-1}{90} & 0 & 0 \\
0 & 0 & \frac{-1}{90} & \frac{4}{45} & \frac{2}{45} & \frac{2}{45} \\
\frac{-1}{90} & 0 & 0 & \frac{2}{45} & \frac{4}{45} & \frac{2}{45} \\
0 & \frac{-1}{90} & 0 & \frac{2}{45} & \frac{2}{45} & \frac{4}{45}
\end{bmatrix}$$

Table 2. *B* **matrix**

$$\begin{bmatrix}
\frac{Y_{23}}{15} & \frac{-Y_{31}}{30} & \frac{-Y_{12}}{30} & \frac{-Y_{23}+Y_{31}}{30} & \frac{Y_{23}}{30} & \frac{Y_{12}-Y_{23}}{15\ \ 30} \\
\frac{-Y_{23}}{30} & \frac{Y_{31}}{15} & \frac{-Y_{12}}{30} & \frac{(Y_{23}-Y_{31})}{15\ \ 30} & \frac{(-Y_{31}+Y_{12})}{30\ \ 15} & \frac{Y_{31}}{30} \\
\frac{-Y_{23}}{30} & \frac{-Y_{31}}{30} & \frac{Y_{12}}{15} & \frac{Y_{12}}{30} & \frac{Y_{31}-Y_{12}}{15\ \ 30} & \frac{(4\ Y_{12}+2\ Y_{23})}{5\ \ 15} \\
\frac{Y_{23}}{10} & \frac{Y_{31}}{10} & \frac{Y_{12}}{30} & \frac{-4}{15}\ Y_{12} & \frac{(2\ Y_{31}+4\ Y_{12})}{15} & \frac{(4\ Y_{12}+2\ Y_{23})}{5\ \ 15} \\
\frac{-Y_{23}}{30} & \frac{Y_{31}}{10} & \frac{1}{15}\ Y_{12} & \frac{(4\ Y_{23}+2\ Y_{31})}{15} & \frac{4}{15}\ Y_{23} & \frac{(2\ Y_{12}+4\ Y_{23})}{15} \\
\frac{Y_{23}}{10} & \frac{-Y_{31}}{30} & \frac{-1}{10}\ Y_{12} & \frac{(2\ Y_{23}+4\ Y_{31})}{15} & \frac{(4\ Y_{31}+2\ Y_{12})}{15} & \frac{-4}{15}\ Y_{31}
\end{bmatrix}$$

$Y_{12} = (Y_1 - Y_2);\ Y_{23} = (Y_2 - Y_3);\ Y_{31} = (Y_3 - Y_1)$

B MATRIX

Assembly of these element matrices can be performed using Boolean operations as in structural analysis.[9]

Numerical Integration of Equations (13) and (14)

The kernel F appearing in Eqs. (13) and (14) is analytic over the area of a triangle lying completely within the forward Mach lines. Hence in these circumstances a numerical integration method of Gaussian quadrature type may be used. However, for elements partially cut by Mach lines, F has an inverse square root singularity. This singularity can be removed by truncating a small width along the Mach line, and transforming this strip element into a characteristic coordinate system. A closed form integration can then be performed over the strip and a numerical integration over the remaining part of the element. A more detailed description is given in Ref. 10.

Numerical Results and Discussion

In this work a 45° delta wing, a 60° delta wing and an AGARD swept trapezoidal wing have been considered. Quadratic interpolation for the velocity potential has been used throughout.

Figure 3 compares qualitatively the pressure distributions predicted using Mach box and consistent approaches in a steady flow at constant incidence over a 60° delta wing at Mach 1.5. Avoidance of jagged leading edges and Mach lines and introduction of piecewise continuous downwash distribution have resulted in smooth pressure distribution even though far fewer elements are used in the consistent approach.

Generalized unsteady aerodynamic force coefficients for a 45° delta wing are shown in Table 3. The modes considered are heave, quadratic spanwise bending and pitching about the apex at $M = 1.5$ and $K = 1.02$. With five triangular elements in the chordwise direction, aerodynamic terms are in very good

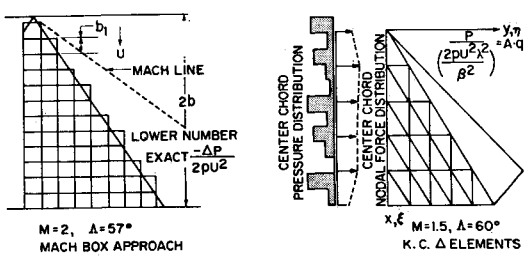

Fig. 3. Comparison of pressure distribution on a delta wing at constant angle of attack in steady flow.

Table 3. Comparison of unsteady aerodynamic coefficients for a delta wing.

GENERALIZED FORCES	EXACT 3D THEORY		FDL-TR-68-30 20 M BOXES ALONG CR		PRESENT 5 FINITE ELEMENTS		COMPARISON WITH EXACT THEORY	
Q_{ij}	Re	Im	Re	Im	Re	Im	AMP. %	PHASE DIFF IN ANGLE
Q_{11}	-0.0655	-0.2944	-0.0636	-0.301	-0.068	-0.304	-2.0	0.41°
Q_{12}	-0.008	-0.0546	-0.0076	-0.553	-0.009	-0.0544	-1.16	0.5°
Q_{13}	-0.3308	-0.1475	-0.3317	-0.1516	-0.338	-0.145	-0.69	0.5°
Q_{21}	-0.0233	-0.0674	-0.0222	-0.0684	-0.0254	-0.0674	-0.83	1.0°
Q_{22}	-0.0033	-0.0237	-0.0031	-0.0243	-0.0037	-0.0209	-0.24	1.66°
Q_{23}	-0.0772	-0.0278	-0.0777	-0.0299	-0.0785	-0.025	-1.46	1.16°
Q_{31}	-0.0469	-0.1935	-0.0455	-0.1948	-0.0494	-0.20	-0.4	0.33°
Q_{32}	-0.0066	-0.0435	-0.0063	-0.0441	-0.00725	-0.043	-1.25	0.50°
Q_{33}	-0.219	-0.112	-0.2197	-0.1142	-0.226	-0.1115	-0.814	0.67°

AR = 4.0, M = 1.5, k = 1.02, Λ = 45°
WING MODES $f_1 = 1_{HEAVE}$; $f_2 = \eta^2_{BEND}$; $f_3 = x_{PITCH}$

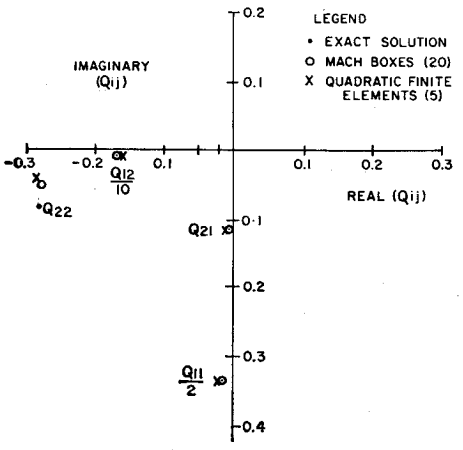

Fig. 4. Vector plot of generalized forces in table 4.

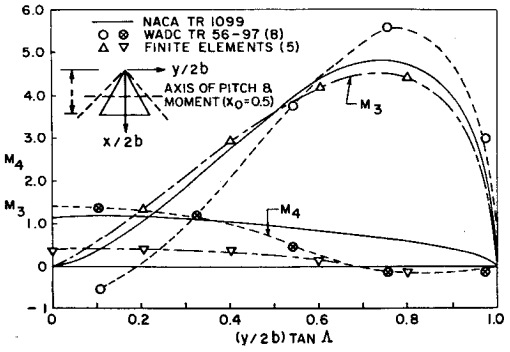

Fig. 6. Spanwise pitching moment distribution for triangular wing in uniform pitching motion about an axis through the midchord ($\Lambda = 60°$, $M = 1.5$, k (0.2).

agreement with the exact theory. Comparable accuracy has been obtained in the Mach box scheme[8] with 20 elements on the center chord and using a quadratic integrating scheme for downwashes in the singular box elements. Table 4 and Fig. 4 show generalized aerodynamic forces for a 60° delta wing in heave and pitching oscillation at $M = 1.5$ and reduced frequency $k = 0.4$. In this case the leading edges are subsonic. The first entries in the finite element column correspond to the linear expression of velocity potential while the second entries are obtained from the quadratic expression of the potential. Although at first sight, the smaller components appear to be poor, the quadratic expression yields very much improved results in terms of amplitude and phase. Figure 4 shows for this wing the vector plot of the generalized coefficients. Even in the subsonic leading edge case five triangles in the center chord yield relatively good accuracy. A similar comparison of results from linear and quadratic expressions in the steady and supersonic leading edge cases (in the first two examples) did not show any appreciable change.

Figure 5 shows spanwise lift distribution on a 60° delta wing in pitching oscillation at $M = 1.5$ and $k = 0.2$. The real part of the lift is in very good agreement with exact theory. The imaginary part which is very much smaller in magnitude does not agree so well. For the same case the spanwise moment distributions are shown in Fig. 6. The real part of the moment distribution is seen to be in close agreement with the exact value. The imaginary part of the moment distribution from exact theory, as shown in Ref. 6, does not seem to be compatible with the imaginary part of lift distribution since it should change sign beyond 0.65 of the span. In addition, the real part of the moment distribution from the Mach box method (Ref. 6) is seen to be far removed from the exact value although the corresponding lift distribution was seen to be very good (See Fig. 5). This indicates that the fluctuating pressure distributions from Mach box theory may yield good results in an average manner, but that local effects will be amplified in the weighted summing arising from moment or distortion mode integrations and cause poor results for these.

Finally, an AGARD trapezoidal wing with and without out-board control surfaces is treated. Table 5 shows generalized coefficients for heaving and pitching of the wing, and rotation of the control surface. The real parts of the coefficients from four (4) finite elements and twenty-four (24) Mach boxes[8] which dominate the forces, compare well. An additional example for the same wing but without control surface, in Table 6 and Fig. 7, is compared with Ref. 13. Figure 7 shows the number of elements, matrix size and the vector plot of the results from Mach box and finite element modeling. The results from fewer elements compare very well with the Mach box method.

Table 4. Comparison of unsteady aerodynamic coefficients for a delta wing $\Lambda = 60°$, $M = 1.5$, $k = 0.4$

Q_{ij}	EXACT 3-D		FDL-TR-68-30 20 BOXES (A)		5 FINITE ELEMENTS (B)	
	REAL	IMAGINARY	REAL	IMAGINARY	REAL	IMAGINARY
Q_{11}	-0.0299	-0.6744	-0.0302	-0.6782	-0.034* -0.0400	-0.592* -0.6622
Q_{12}	-1.7113	-0.0833	-1.7060	-0.0922	-1.50* -1.6658	-0.063* -0.054
Q_{21}	-0.0076	-0.1108	-0.0066	-0.1071	-0.0078* -0.0100	-0.107* -0.113
Q_{22}	-0.2817	-0.0853	-0.2718	-0.0531	-0.272* -0.286	-0.040* -0.041

* WITH LINEAR EXPRESSION FOR VELOCITY POTENTIAL

WING MODES: $f_1 = 1$, $f_2 = X - C_R/2$

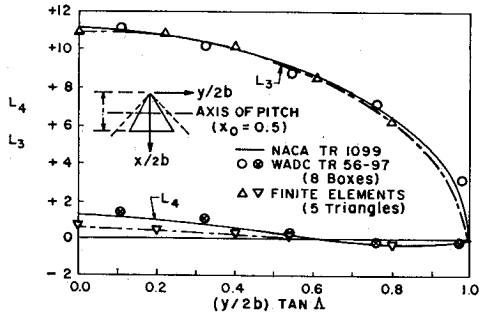

Fig. 5. Spanwise lift distribution for a triangular wing in uniform pitching motion about an axis through the midchord ($\Lambda = 60°$, $M = 1.5$, $k = 0.2$).

Table 5. AGARD swept wing with outboard control surfaces.

GENERALIZED COEFFICIENTS	AFFDL-TR-68-30 4 BOXES		24 BOXES		4 FINITE ELEMENTS ALONG CHORD	
	REAL	IMAGINARY	REAL	IMAGINARY	REAL	IMAGINARY
Q12	-3.011	-1.469	-2.891	-1.456	-2.72	-2.14
Q13	-0.2843	-0.0565	-0.3034	-0.0144	-0.254	-0.00128
Q22	-3.03	-1.813	-2.835	-1.798	-2.7	-2.74
Q33	+0.0551	-0.005	-0.035	-0.0024	-0.0208	-0.00158

WING MODES: $f_1 = 1.0$, $f_2 = x$, $f_3 = 0$

CONTROL SURFACE MODES: $f_1 = 1.0$, $f_2 = x$, $f_3 = 13.63 + -0.3424Y$

M = 2.0

ASPECT RATIO = 1.45

K = 0.8065

Table 6. Comparison of generalized forces for AGARD swept wing.

GENERALIZED FORCES Q_{ij}	FDL-TR-67-104 17 M BOXES		4 FINITE ELEMENTS 5 POINTS	
	Re	Im	Re	Im
Q_{11}	-0.1529	+3.290	-0.131	+3.26
Q_{12}	-0.3306	+0.595	-0.346	0.645
Q_{21}	2.501	1.13	2.42	1.35
Q_{22}	0.5708	1.19	0.569	1.298

M = 2.0, k = 1.4
WING MODES :- f_1 = 1.0 (HEAVE)
f_2 = X - 0.5 CR (PITCH)

17 M BOXES PER CENTER CHORD	VS	4 TRIANGULAR ELEMENTS PER CENTER CHORD

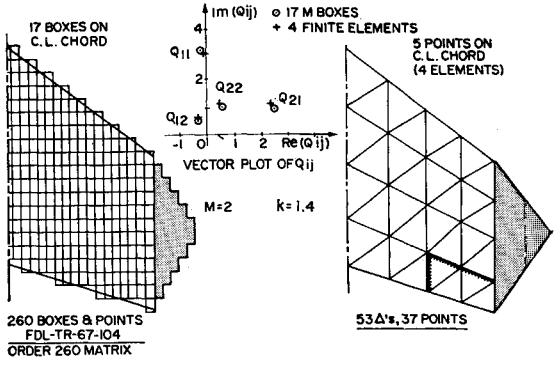

Fig. 7. AGARD trapezoidal wing.

Conclusions

The present work has described the evaluation of unsteady supersonic aerodynamic coefficients which are kinematically consistent with structural analysis approaches. A number of examples shown in this paper indicate much improved local, as well as over-all results from far less effort. Accuracy and/or economic gains will be obtained for complex deformation modes, general wing shapes and subsonic trailing edges cases by the application of quadratic interpolation functions for both velocity potentials and displacements. Additional advantages of the method are: 1) Operations are more consistent with structural analysis, hence are potentially a good approach for flutter analysis and aeroelastic optimization, transient load estimation, etc. 2) Wing edges are better matched and result in more regular pressure distribution. 3) Computer programing is simplified and is unified with the structural system.

Although not explored so far in the present work the ability to define grid points independently on the wing and in the diaphragms offers the possibility of optimizing their distribution. Conceptually, there is no barrier to the extension of the basis of the present approach to more complex problems including nonplanar and interfering surfaces.

References

[1] Garrick, I. E. and Rubinow, S. I., "Flutter and Air-Force Calculations for an Airfoil in a Two-Dimensional Supersonic Flow," R-846, 1946, NACA.

[2] Garrick, I. E. and Rubinow, S. I., "Theoretical Study of Air Forces on an Oscillating or Steady Thin Wing in a Supersonic Main Stream," R-872, 1947, NACA.

[3] Ashley, H., Widnall, S., and Landhal, M. T., "New Directions in Lifting Surface Theory," *AIAA Journal*, Vol. 3 No. 1, Jan. 1965, pp. 3–16.

[4] Bisplinghoff, R. L. and Ashley, H., "Principles of Aeroelasticity," Wiley, New York, 1962, pp. 136.

[5] Cunningham, H. J., "Improved Numerical Procedure for Harmonically Deforming Lifting Surfaces from the Supersonic Kernel Function Method," *AIAA Journal* Vol. 4, No. 11, Nov. 1966, pp. 1961–1968.

[6] Zartarian, G. and Hsu, P. T. "Theoretical Studies on the Prediction of Unsteady Supersonic Airloads on Elastic Wings," Pts. I and II, Wright Air Development Center, Wright Patterson Air Force Base, Ohio. TR 56–97, 1955.

[7] Moore, M. T. and Andrew, L. T., "Unsteady Aerodynamics for Advanced Configurations," Part IV—"Application of Supersonic Mach Box Method to Intersecting Planar Lifting Surfaces," FDL-TDR-64-152, May 1965; also Part VI—"Supersonic Mach Box Method Applied to T-Tails, V-Tails and Top Mounted Tails," May 1969,

[8] Donato, V. W. and Huhn, C. R. J., "Supersonic Unsteady Aerodynamics for Wings with Trailing Edge Control Surfaces and Folded Tips," FDL-TR-68-30, Aug. 1968,

[9] Argyris, J. H., "Continua and Discontinua," *Proceedings of the Air Force Conference on Matrix Methods Structural Mechanics*, 1965, Wright-Patterson Air Force Base, Dayton, Ohio.

[10] Kariappa, "Kinematically Consistent Unsteady Aerodynamic Coefficients in Supersonic Flow," Pts. I and II—TN-9; National Aeronautical Lab., India, March 1968, also see, *The International Journal for Numerical Methods*, Vol. 2, No. 4, Oct. 1970, pp. 495–507.

[11] Kariappa and Somashekar, B. R., "Application of Matrix Displacement Methods in the Study of Panel Flutter," *AIAA Journal*, Vol. 7, No. 1, Jan. 1969, pp. 50–53.

[12] Kariappa and Smith, G. C. C., "Further Developments in Consistent Aerodynamic Coefficients in Supersonic Flow," IR&D Program of Bell Aerospace Co., Oct. 1969, unpublished.

[13] Olsen, J. J., "Demonstration of a Supersonic Box Method for Unsteady Aerodynamics of Non-planar Wings," FDL-TR-67-104 Pts. I and II, Feb. 1969, AFFDL Wright-Patterson Air Force Base, Ohio.